Hindawi
Journal of Spectroscopy
Volume 2020, Article ID 8818709, 11 pages
https://doi.org/10.1155/2020/8818709

Research Article

The Vibrational Spectroscopy of the Valence Bonds of Cu-Doped TiO_2 Using Electronegativity Principle Quantitative Calculations

Ji-Kang Yan, Jun-Yu Chen, and Guo-You Gan

Kunming University of Science and Technology, Kunming, China

Correspondence should be addressed to Ji-Kang Yan; scyjk@qq.com

Received 4 September 2020; Accepted 12 December 2020; Published 28 December 2020

Academic Editor: Stephen Cooke

Copyright © 2020 Ji-Kang Yan et al. This is an open access article distributed under the Creative Commons Attribution License, which permits unrestricted use, distribution, and reproduction in any medium, provided the original work is properly cited.

The purpose of this study is to investigate the influence of Cu on TiO_2 phase transformation and regioselectivity. TiO_2 samples doped with different amounts of Cu^{2+} ions were synthesized by the sol-gel method. The phase and vibrational mode were characterized by X-ray diffraction (XRD), Fourier infrared spectroscopy (FTIR), and transmission electron microscope (TEM). The XRD phase analysis shows that the lattice parameters have not changed after Cu incorporation. In addition, the content of rutile increased obviously after Cu doping. This indicated that the addition of Cu obviously promoted the transformation from anatase phase to rutile phase. The vibration frequencies were calculated based on the principle of electronegativity. All types of bonds were qualitatively and quantitatively analyzed. The content of Ti_A-O, Ti_R-O, and H-O in the undoped TiO_2 samples is 23.87%, 16.30%, and 7.41%, respectively. In the same way, the content of Ti_A-O, Ti_R-O, H-O, Cu^i_A-O, and Cu^i_R-O in the 2.5 mol% Cu-doped TiO_2 samples is 21.23%, 18.56%, 7.34%, and 0.98%, respectively. For the 5 mol%Cu-doped TiO_2 samples, the content of Ti_A-O, Ti_R-O, H-O, Cu^i_A-O, Cu^i_R-O, Cu^s_A-O, and Cu^s_R-O is 18.75%, 20.11%, 7.47%, 2.56%, 3.9%, 1.55%, and 2.35%, respectively. Cu was not present at substitutional sites in the 2.5 mol% doped sample, but Cu was present in the 2.5 mol% doped sample. It is indicated that Cu was more likely to exist in the form of interstitial position in the TiO_2 lattice, with the number of Cu atoms in the interstitial position reaching saturation, and this forced Cu to replace Ti. The TEM shows that the stripes of different periods and orientations overlapped each other to form the Moiré patterns. In addition, the diffraction patterns of the Moiré image were slightly different from that of the matrix. The Cu replaced Ti position and the Cu atoms mixed into interstitial sites in the TiO_2 lattice. The theoretical calculation was consistent with the experimental results.

1. Introduction

The advantages of titanium dioxide include nontoxic, stable chemical properties and high photocatalytic activity [1]. However, the low quantum yield and difficulty in separation and recovery under visible light irradiation limit its further development as a photocatalyst [2]. To improve the photo efficiency of the electronic process as well as the response into the visible part of the spectrum, TiO_2 doping with noble metal doping [3], composite semiconductors [4], and transition metal doping [5] have been widely employed. In addition, the effect of doping on the activity also depends on other factors, such as the method of doping and the concentration of dopant [6].

Recently, Cu-doping has been increasingly investigated as a dopant for titania. Byrne et al. [7] studied Cu-doped rutile and anatase. The results show the formation of charge compensating oxygen vacancies and a Cu^{2+} oxidation state. D. M. Tobaldi [8] studied Cu–TiO_2 hybrid nanoparticles exhibiting tunable photochromic behavior. This retards the anatase-to-rutile phase transition and titania domain growth through a grain-boundary pinning mechanism. These hybrid nanoparticles show tunable photochromic behavior under both UVA and visible light. However, there are few works of literatures about the qualitative and quantitative analysis of Cu-doped TiO_2. We will conduct a quantitative and qualitative analysis of Cu-doped TiO_2 by electronegative principle. In our previous work, the (Fe, N) Co-doped TiO_2

infrared spectrum is calculated by the principle of electronegativity [8] and demonstrated qualitatively that N enters the TiO_2 lattice and substitutes O, forming the Ti-N structure; Fe iron enters the TiO_2 lattice and substitutes Ti, forming the Fe-O structure. When both N and Fe substitutions occurred simultaneously, they resulted in the Fe-N structure. These valence bond structures and the original Ti-O bond structure in anatase and rutile together formed a wide band of IR absorption, which was consistent with the actual IR test results.

In this work, Cu-doped and undoped TiO_2 samples were prepared with the sol-gel method. The crystalline phase and IR spectra of the samples were characterized by X-ray diffraction and Fourier infrared spectroscopy (FTIR). The XRD phase analysis showed that the addition of Cu promoted the transformation of anatase phase to rutile phase, but only at the level of qualitative analysis. By infrared spectroscopy and combining the principle of electronegativity, the doping of Cu was further quantitatively analyzed.

2. Experimental Details

2.1. Sample Preparation. The formula A was prepared by mixing 0.982 g of copper acetate and 16 mL of distilled water, and the formula B was prepared by mixing 1.585 g of citric acid and 16 ml of distilled water. After stirring at 50°C for 5 min, formula B was dropped into the prepared formula A. 2 ml of Tetrabutyl titanate and 16 ml of 30 mol% sodium hydroxide solution was added to the mixture of formula A and B, which was stirred at 25°C for 1 hour. Finally, the solution was put into a vacuum drying oven for 60°C and 6 hours. The formed solid was ground to make a powder.

2.2. Characterization. The Cu-doped and undoped TiO_2 systems were characterized by FT-IR, XRD, and TEM, and the Instrument parameters as shown in Table 1.

2.3. Experiment Principles. The motion of two particles under interaction is the relative motion of one particle relative to another. At this point, the quality of the quality point should be changed to the reduced mass [9–13]. For the convenience of calculation, the atoms of the bond can be regarded as the interaction between the particle points. The reduced mass μ could be expressed as follows:

$$\frac{1}{\mu} = \frac{1}{m_1} + \frac{1}{m_2} = \frac{m_1 + m_2}{m_1 m_2}. \quad (1)$$

In equation (1), $\mathbf{m_1}$ and $\mathbf{m_2}$ are relative atomic mass. The $\mathbf{m_{Ti}}$ is 47.87, $\mathbf{m_{Cu}}$ is 55.845, and $\mathbf{m_O}$ is 16.00. In practice, nonharmonic motion is dominant. The anharmonic vibrational problem is usually solved by using second-order perturbation theory with a harmonic reference wave function, often with some treatment of Fermi resonances [10]. The geometrical component of anharmonic motion is considered as a combination of multiple simple harmonic motions. According to classical mechanics, the stretching force constant k and frequency υ satisfy the following relation [14–17]:

$$\nu = \frac{1}{2\pi}\sqrt{\frac{k}{\mu}}. \quad (2)$$

In equation (2), the unit of υ is cm^{-1}. The VSCF (vibrational density of states) can easily quantize to a simple harmonic oscillator. In the VSCF method, the analysis of anharmonic interaction comprises coupling between different modes of vibration. The VSCF algorithm is based on the approximation of separability and the total vibrational wave function is described by a product of single mode wave functions [18–21]. By calculating the simple harmonic motion in a single direction, Jun-yu Chen [13] proposed the following relationship between the force constants and electronegativity:

$$k = mN\left(\frac{XaXb}{d^2}\right)^{3/4}. \quad (3)$$

In equation (3), **k** is the stretching force constant, **d** is the bond length, **N** is the bond order, and **Xa** and **Xb** are the electronegativities of the atoms at both ends of the bond (k unit: dynes/cm10^{-5}, d unit: Å). The values of m are 1.84 for stable molecules [22–25]. The bond order N could be calculated as follows: N= (total number of electrons in a stable structure - total number of valence electrons)/2; the calculation yields a bond order of 0.5. By looking up the electronegativity table, the following values are obtained [26]: $X_{Ti} = 1.54$, $X_O = 3.44$, and $X_{Cu} = 1.90$.

3. Results and Discussion

3.1. TiO_2 Molecular Structure Model. Figure 1 is the structural model of TiO_2. From the periodic arrangement, it can be seen that it constitutes multiple oxygen octahedral structure units, and so only the model of a single cell structure needs to be discussed. The basic unit in the structure of both rutile and anatase TiO_2 is oxygen octahedral. The subscript of the element symbol represents the position of this atom. The number between the two atoms represents the bond length. For instance, Ti_A represents that Ti atom is in Titanium lattices of anatase TiO_2.

3.2. Cu-Doped TiO_2 Structure Model. Figures 2(a) and 2(b) show that in the anatase, Cu atoms replace Ti atoms in the substitutional sites or occupy the interstitial sites. Figures 2(c) and 2(d) show that in the rutile, Cu atoms are in the substitutional sites and interstitial sites. Doping substitutional and interstitial sites are constructed by using SDD (selection of configuration types in Gaussian optimization) configuration, GaussView, and Gaussian09w[27]. The information on bond length and the position of each atom is shown in Figure 2. The dashed line between Cu and O indicates that Cu can form O-Cu-O with two O atoms and can also form Cu-O with only an O atom. The lower right corner of the symbol indicated that atomic location number. The numbers between the two atoms indicate that the bond distance between two atoms (unit: Å).

Table 1: Instrument parameters.

Equipment name	Parameters
FT-IR (Fourier transform infrared spectroscopy)	Spectral range: 4000–400 cm^{-1} Max resolution ratio: 0.0035 cm^{-1} SNR (Signal to Noise Ratio): 50000 : 1
XRD	The sample size: $\varphi \leq 350$ mm Export: asc, raw, dat, and so on.
TEM	Magnification times: 80~1000k times Resolution ratio: 0.15~0.18 nm Acceleration voltage: 200 kV

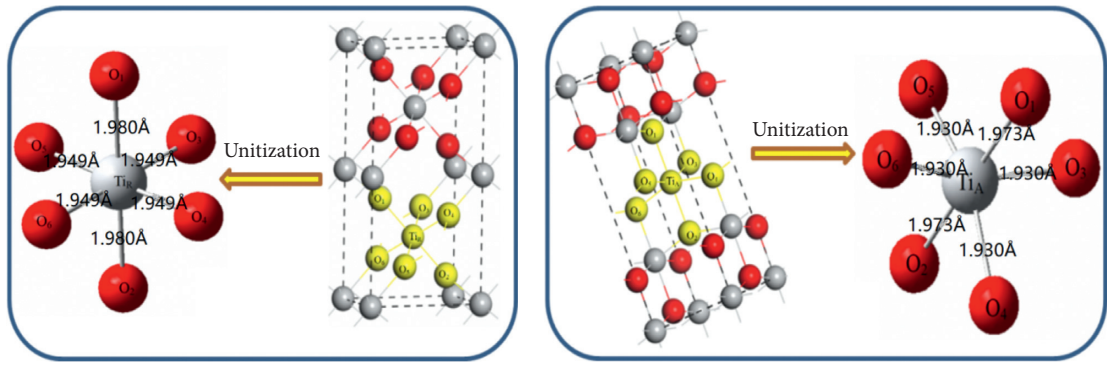

(a) (b)

Figure 1: The structural model of TiO_2; (a) the structural model of rutile; (b) the structural model of anatase.

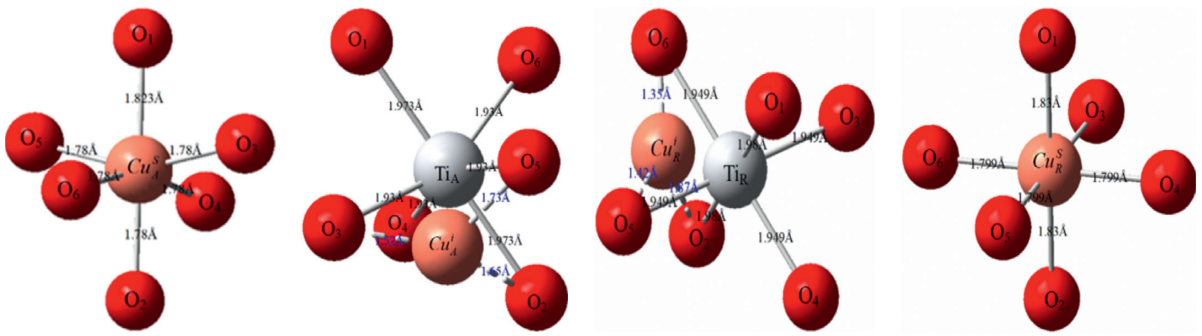

(a) (b) (c) (d)

Figure 2: Cu-doped TiO_2 structure model; (a) Cu replaced substitutional sites in the anatase; (b) Cu occupied interstitial sites in the anatase; (c) Cu replaced interstitial sites in the rutile; (d) Cu occupied substitutional sites in the rutile.

3.3. X-Ray Diffraction Analysis. XRD patterns of undoped TiO_2, 2.5 mol% Cu-doped TiO_2, and 5 mol% Cu-doped TiO_2 by the sol-gel technique are shown in Figure 3. The calcination temperature of Cu-doped TiO_2 samples at 550°C. According to the standard diffraction cards [15], the results show that only existing rutile and anatase phases in the TiO_2 and Cu-doped TiO_2 samples, because brookite phase is unstable, there existed transition from brookite to anatase [27–29]. In Figure 3, four peaks corresponding to $(101)_A$, $(004)_A$, $(200)_A$, and $(211)_A$ planes of TiO_2 anatase phase are observed (PDF #21–1272); the formation of the rutile phase is confirmed by matching five peaks corresponding to $(110)_R$, $(101)_R$, $(111)_R$, $(211)_R$, and $(220)_R$ planes which match with data card (PDF #21–1276). It can be found that the content of rutile increased obviously after Cu doping. This indicates that the addition of Cu obviously promoted the transformation from anatase phase to rutile phase. In the section of the infrared spectrum, we will use the electronegativity principle to analyze it quantitatively. The lattice parameters of samples are calculated from the XRD patterns shown in Table 2. The addition of Cu cannot change the lattice parameters. This evidence is considered that a greater portion of the Cu^{2+} ions is well-incorporated into the anatase and rutile TiO_2 lattice [17]. Through contact to bulk anatase and rutile TiO_2, a small change in lattice constant has been observed for the Cu-doped TiO_2 samples as shown in Table 2. The reason for this might be due to the tensile strain in the lattice [30].

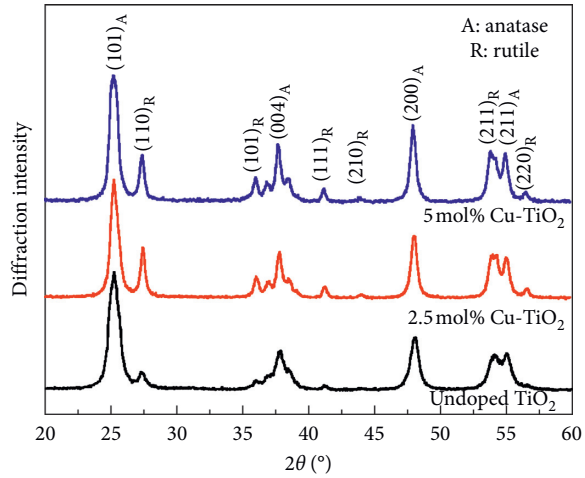

Figure 3: XRD patterns of the Cu-doped TiO_2 samples with different doping concentrations at calcination temperature (550°C).

Table 2: The lattice parameters of the Cu-doped TiO_2 samples with different doping concentrations.

	Anatase					Rutile					
Cu^{2+} (mol%)	d_{101} (Å)	d_{004} (Å)	d_{200} (Å)	$a = b$ (Å)	c (Å)	d_{101} (Å)	d_{101} (Å)	d_{101} (Å)	d_{101} (Å)	$a = b$ (Å)	c (Å)
0	3.517	2.373	1.891	3.782	9.493	3.741	2.869	2.481	1.784	4.594	2.953
3	3.516	2.374	1.893	3.787	9.497	3.744	2.865	2.487	1.787	4.597	2.956
5	3.514	2.376	1.894	3.785	9.496	3.743	2.861	2.482	1.788	4.596	2.957

3.4. Full Wave Number Section of Infrared

3.4.1. Spectroscopy. Figure 4 shows the full wavenumber section of the infrared spectra of the undoped and Cu-doped TiO_2 samples. Ti_A-O is Ti-O bonds in anatase. Ti_R-O is Ti-O bonds in rutile. Cu^i_A-O is Cu replaced interstitial sites in the anatase. Cu^i_R-O is Cu occupied interstitial sites in the rutile. Cu^s_A-O is Cu replaced substitutional sites in the anatase. Cu^s_R-O is Cu occupied substitutional sites in the rutile. Not all structures are symmetrical, and most of the TiO_2 crystal structures are asymmetric. It caused the bond length to fluctuate within a range [31–33]. In the actual situation, the crystal structure of Cu-doped and undoped TiO_2 is continuously optimized. According to the electronegativity principle [34], the calculation results of all vibration frequencies are calculated in Table 3. In this part, by conducting full-spectrum analysis and predicting the patterns of Cu doping, Figure 4(b) indicates that the absorption peaks of Ti_A-O, $Cu_A{}^s$-O, and Cu^i_A-O are similar. When the doping amount of Cu is 2.5 mol%, the absorption peaks of Ti_A-O are narrower. Meanwhile, the absorption peaks of Cu^i_A-O and Cu^s_A-O appear in anatase lattice. Figure 4(c) indicates that when the doping amount of Cu is 5 mol%, the absorption peaks of Cu^i_R-O and Cu^s_R-O are to appear in rutile lattice. The transmittance of Cu-O bond decreased from $T = 0.74$ to $T = 0.38$. Meanwhile, the absorption peaks of Ti_R-O are also narrower. It is predicted that in the rutile and anatase phases, a part of Cu and O atoms by interstitial solid solution to form Cu-O bond, and another part of Cu replaces Ti atoms by substitutional solid solution to form Cu-O bond with O atoms in the TiO_2 lattice. In the next part, we will quantitatively analyze and prove it.

3.5. Low Wave Number Section of Infrared Spectroscopy ($400\,cm^{-1}$~$1800\,cm^{-1}$).

The d_A is the substituted value into formula (3), and the stretching vibration frequencies of Ti-O in anatase and rutile were calculated by electronegativity principle. In Figure 5, the values of the ν_{TiA-O} (orange) are 454.25 cm^{-1}, 508.54 cm^{-1}, 548.17 cm^{-1}, 580.35 cm^{-1}, 620.9 cm^{-1}, 670.1 cm^{-1}, 1114.3 cm^{-1}, and 1563.4 cm^{-1}, respectively. The values of the ν_{TiR-O} (blue) are 716.7 cm^{-1}, 765.65 cm^{-1}, 823.66 cm^{-1}, 1395.6 cm^{-1}, 1459.5 cm^{-1}, and 1513.7 cm^{-1}, respectively. The values of the ν_{H-O} (green) were 1638.3$cm^{-1}$and 1712.9 cm^{-1}. After the position of various bonds was determined, we would use the FTIR peak fitting method [35] to analyze it quantitatively. In Figure 5, the proportion of each peak was calculated, the red curve is the fractal fitting calculation, and the black curve is the actual measurement, and the fitting rate is 99.87%. Table 4 counts the content of bonds. It indicated that there were three types of bonds; the content of Ti_A-O, Ti_R-O, and H-O is 23.87%, 16.30%, and 7.41%, respectively. In the 550°C and undoped TiO_2 sample, the number of Ti_A-O bonds is greater than that of Ti_R-O bonds.

Figure 6 shows that the infrared spectra of the 2.5 mol %Cu-doped TiO_2 samples. The fitting rate is 99.95%. The values of the ν_{TiA-O} (orange) are 458.99 cm^{-1}, 509.79 cm^{-1}, 541.21 cm^{-1}, 574.02 cm^{-1}, 623.11 cm^{-1}, 666.94 cm^{-1}, 1574.6 cm^{-1}, and 1114.3 cm^{-1}, respectively. The values of the ν_{TiR-O} (blue) are 710.29 cm^{-1}, 748.65 cm^{-1}, 796.48 cm^{-1}, 848.4 cm^{-1}, 1394.74 cm^{-1}, 1458.5 cm^{-1}, 1503.3 cm^{-1}, and 1537.9 cm^{-1}, respectively. The values of the ν_{H-O} (green) are 1633.4 cm^{-1} and 1680.9 cm^{-1}. At the same time, there are two new bonds, the values of the νCu^i_A-o (dark cyan) are 489.74 cm^{-1} and the values of the

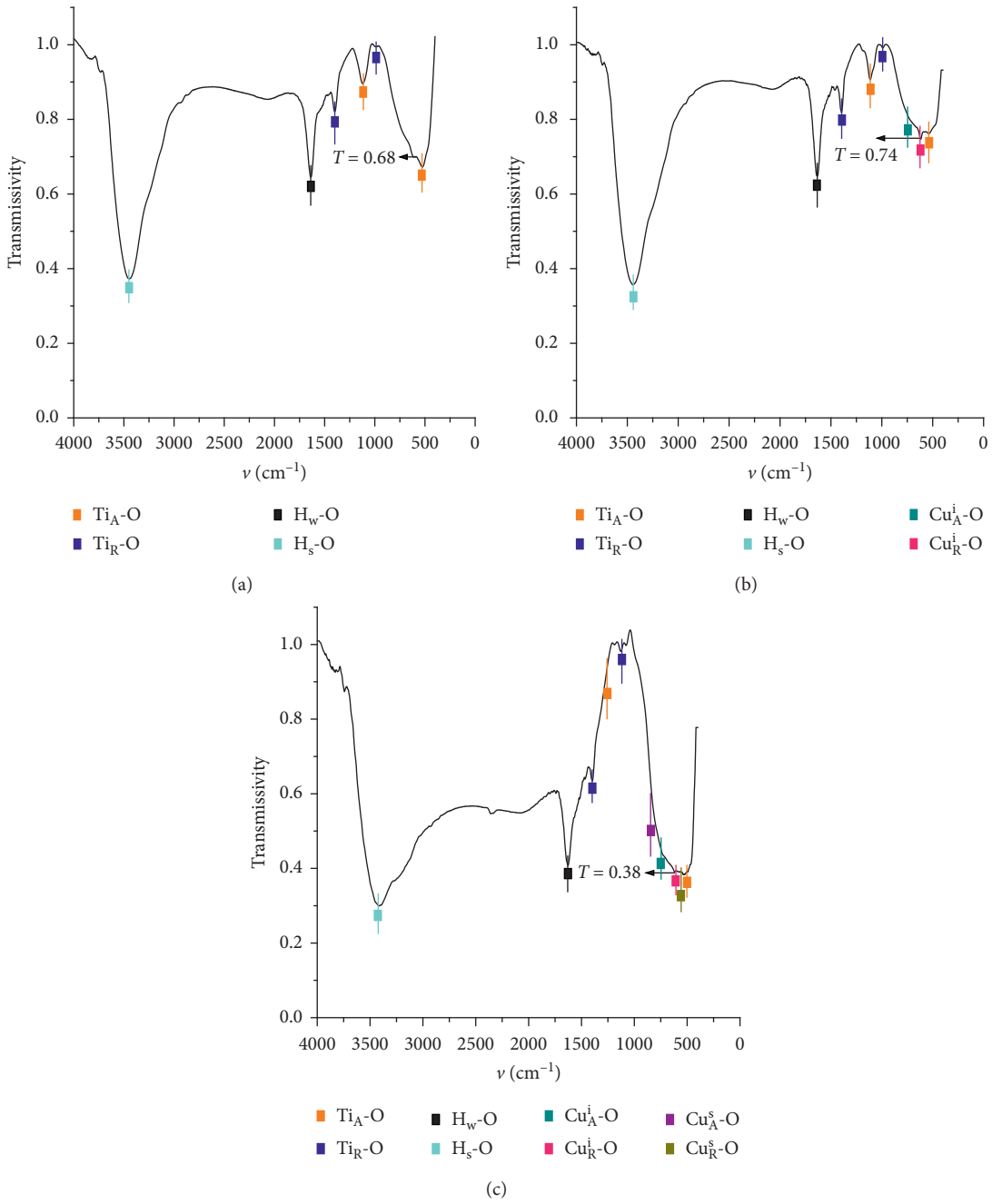

FIGURE 4: Full wave number section of the Infrared Spectra of the Cu-doped TiO_2 samples with different doping concentrations at calcination temperature (550°C).(a) Undoped. (b) 2.5 mol%Cu. (c) 5 mol%Cu.

νCu^i_R-o (pink) are 609.31 cm^{-1}. In Table 5, the content of each peak was counted. It is indicated that there are five types of bonds. The content of Ti_A-O, Ti_R-O, H-O, Cu^i_A-O, and Cu^i_R-O is 21.23%, 18.56%, 7.34%, 0.98%, and 1.34%, respectively. By compared with the undoped TiO_2, the content of Ti_A-O decreased by 2.64%, the content of Ti_R-O increased by 2.26%, and the content of the H-O bond is little changed. It quantitatively proved that the addition of Cu promoted the transformation of the anatase phase to rutile phase.

The infrared spectra of the 5 mol% Cu-doped TiO_2 samples in Figure 7. The fitting rate is 99.75%. The values of the ν_{TiA-O} (orange) are 454.71 cm^{-1}, 489.7 cm^{-1}, 509.93 cm^{-1}, 533.05 cm^{-1}, 579.11 cm^{-1}, 586.76 cm^{-1}, 628.09 cm^{-1}, 671.26 cm^{-1}, 712.85 cm^{-1}, 797.43 cm^{-1}, 843.36 cm^{-1}, 1114.3 cm^{-1}, and 1562.7 cm^{-1}, respectively. The values of the ν_{TiR-O} (blue) are 876.86 cm^{-1}, 922.88 cm^{-1}, 1331.8 cm^{-1}, 1371.2 cm^{-1}, 1393.4 cm^{-1}, 1414.9 cm^{-1}, 1449.4 cm^{-1}, 1478.7 cm^{-1}, 1517.3 cm^{-1}, 1604.6 cm^{-1}, respectively. The values of the ν_{H-O} (green)

Table 3: The vibration frequency range corresponding to the various bonds of undoped and Cu-doped TiO_2 samples.

Sample	Types of the bonds	The bond length d (Å)	Vibration frequency v (cm^{-1})
Undoped TiO_2	Ti_A-O	1.949 Å~1.980	450 cm^{-1}~670 1100 1600
	Ti_R-O	1.930 Å~1.973	710 cm^{-1}~850 1410 cm^{-1}~1550
2.5 mol% Cu-doped TiO_2	Ti_A-O	1.739 Å~1.976	440 cm^{-1}~680 1100 1600
	Ti_R-O	1.627 Å~1.973	680 cm^{-1}~850 1370 cm^{-1}~1650
	Cu^i_A-O	1.327 Å~1.527	450 cm^{-1}~480
	Cu^i_R-O	1.284 Å~1.428	550 cm^{-1}~720
5 mol% Cu-doped TiO_2	Ti_A-O	1.729 Å~1.966	435 cm^{-1}~675 1105 1605
	Ti_R-O	1.627 Å~1.973	680 cm^{-1}~850 1370 cm^{-1}~1650
	Cu^i_A-O	1.327 Å~1.527	450 cm^{-1}~480
	Cu^i_R-O	1.284 Å~1.428	550 cm^{-1}~750
	Cu^s_A-O	1.276 Å~1.958	550 cm^{-1}~740
	Cu^s_R-O	1.364 Å~1.965	450 cm^{-1}~820

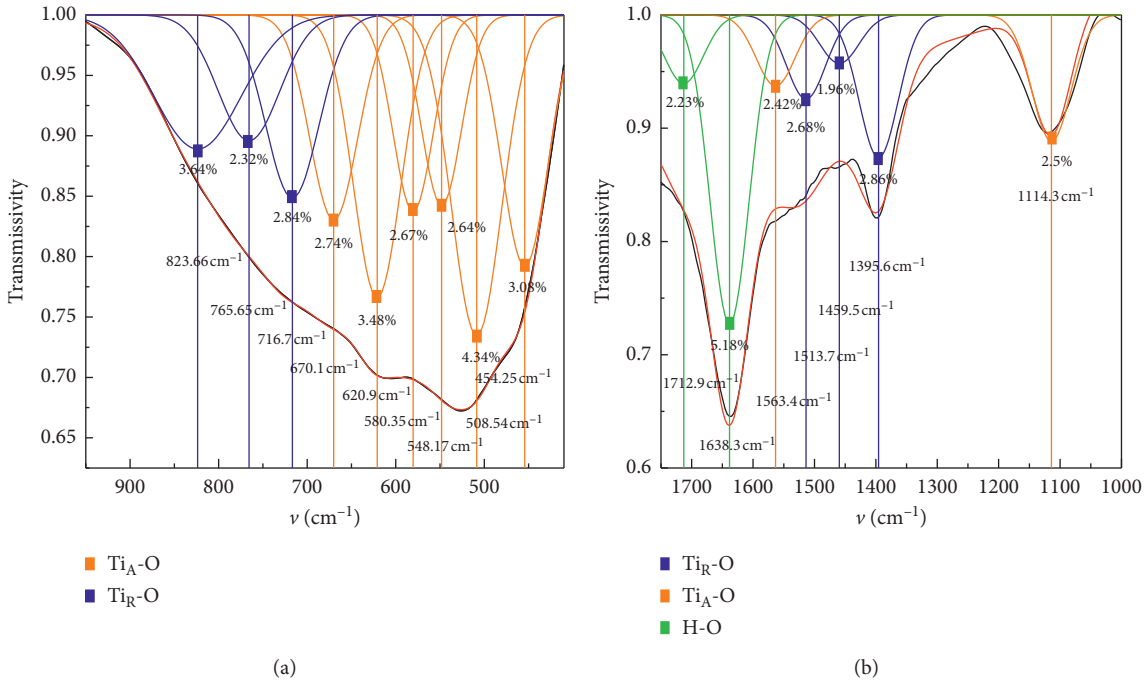

Figure 5: Infrared spectra of the undoped TiO_2 samples at calcination temperature (550°C). (a) 400 cm^{-1}~1000 cm^{-1}; (b) 1000 cm^{-1}~1800 cm^{-1}.

Table 4: Infrared spectra of the undoped TiO_2 samples with the content and vibrational frequency of valence bonds.

The type of bonds	Content (%)	Vibrational frequency (cm^{-1})
Ti_A-O	23.87	1563.4, 1114.3, 670.1, 620.9, 580.35, 548.17, 508.54, and 454.25
Ti_R-O	16.30	1513.7, 1459.5, 1395.6, 823.66, 765.65, and 716.7
H-O	7.41	1712.9, 1638.3

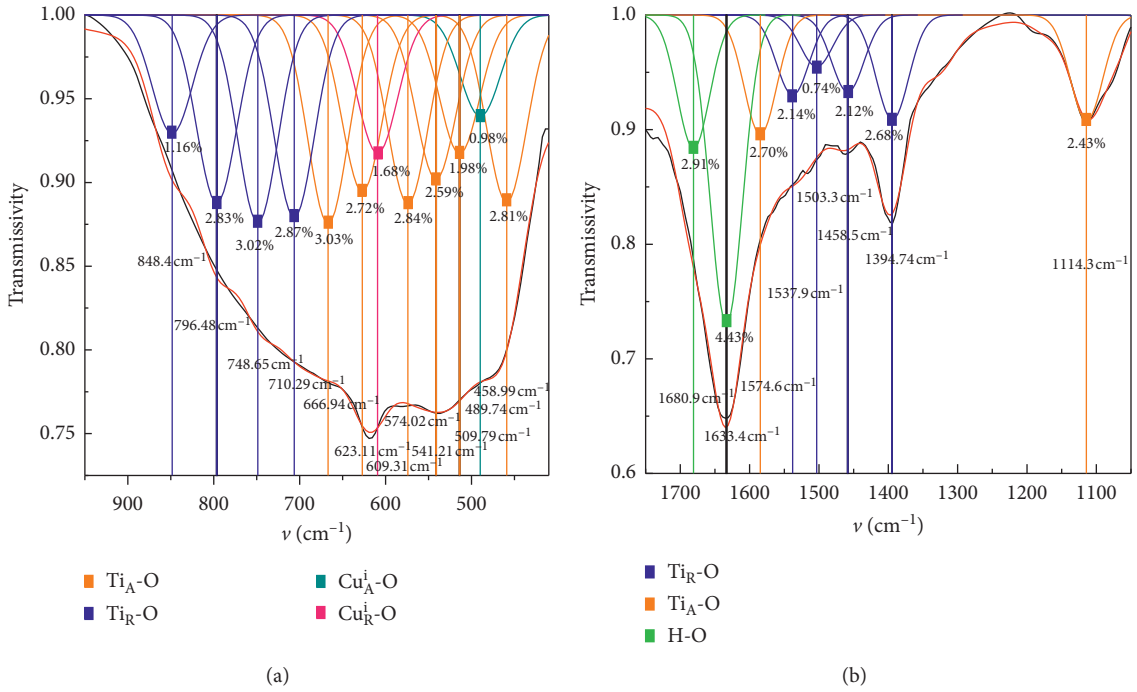

FIGURE 6: Infrared spectra of the 2.5 mol%Cu-doped TiO_2 samples at calcination temperature (550°C). (a) 400 cm^{-1}~1000 cm^{-1}; (b) 1000 cm^{-1}~1800 cm^{-1}.

TABLE 5: Infrared spectra of the 2.5 mol%Cu-doped TiO_2 samples with the content and vibrational frequency of valence bonds.

The type of bond	Content (%)	Vibrational frequency (cm^{-1})
Ti_A-O	21.23	1574.6, 1114.3, 666.94, 623.11, 574.02, 541.21, 509.79, and 458.99
Ti_R-O	18.56	1537.9, 1503.3, 1458.5, 1394.74, 848.4, 796.48, 748.65, and 710.29
H-O	7.34	1680.9 and 1633.4
Cu^i_A-O	0.98	488.74
Cu^i_R-O	1.34	609.31

are 1636.6 $cm^{-1}$and 1673.7 cm^{-1}. The values of νCu^i_A-O (dark cyan) are 549.23 cm^{-1} and 606.28 cm^{-1}. The values of the νCu^s_A-O (purple) are 734.82 cm^{-1} and 1533.5 cm^{-1}. The values of the νCu^s_R-*O* (dark yellow) are 745.97 cm^{-1} and 1287.6 cm^{-1}. When the doping amount of Cu is 2.5 mol%, there are only Cu^i_A-O and Cu^i_R-O, which are interstitial sites. When the doping amount of Cu is 5 mol %, the doping of substitution position occurred. It is shown that interstitial locations are more susceptible to Cu doping because Cu atoms are more inclined to form a spherical shell stable structure in the interstitial position of TiO_2 lattice. Moreover, with the increase of Cu doping content, the clearance position repulsive force increased; when the repulsion is increased to a certain value, Cu atoms of the interstitial position could replace the Ti atoms. Table 6 shows that infrared spectra of the 5 mol% Cu-doped TiO_2 samples of the content of all kinds of bonds. There are seven types of bonds; the content of Ti_A-O, Ti_R-O, H-O, Cu^i_A-O, Cu^i_R-O, Cu^s_A-O, and Cu^s_R-O is 18.75%, 20.11%, 7.47%, 2.56%, 3.9%, 1.55%, and 2.35%. By contrast, the 2.5 mol%Cu-doped TiO_2, the content of Ti_A-O decreased by 2.48%, the content of Ti_R-O increased by 1.55%, the content of Cu^i_A-O increased by 1.58%, the content of Cu^i_R-O increased by 2.56%, and the content of H-O bond is little changed. Because the increase rate of Ti_R-O is lower than that of 2.5 mol%Cu doping, so when Cu doping content is too high, the conversion efficiency of rutile from anatase to rutile would be reduced. In addition, whether the doping amount of Cu is 2.5 mol% or 5 mol%, the content of Cu_R-O is always higher than that of Cu_A-O, and the content of Cu^i-O is more than Cu^s-O. It is represented that in the anatase phase and rutile phase, Cu atoms are more likely to be mixed into interstitial sites and rutile phase.

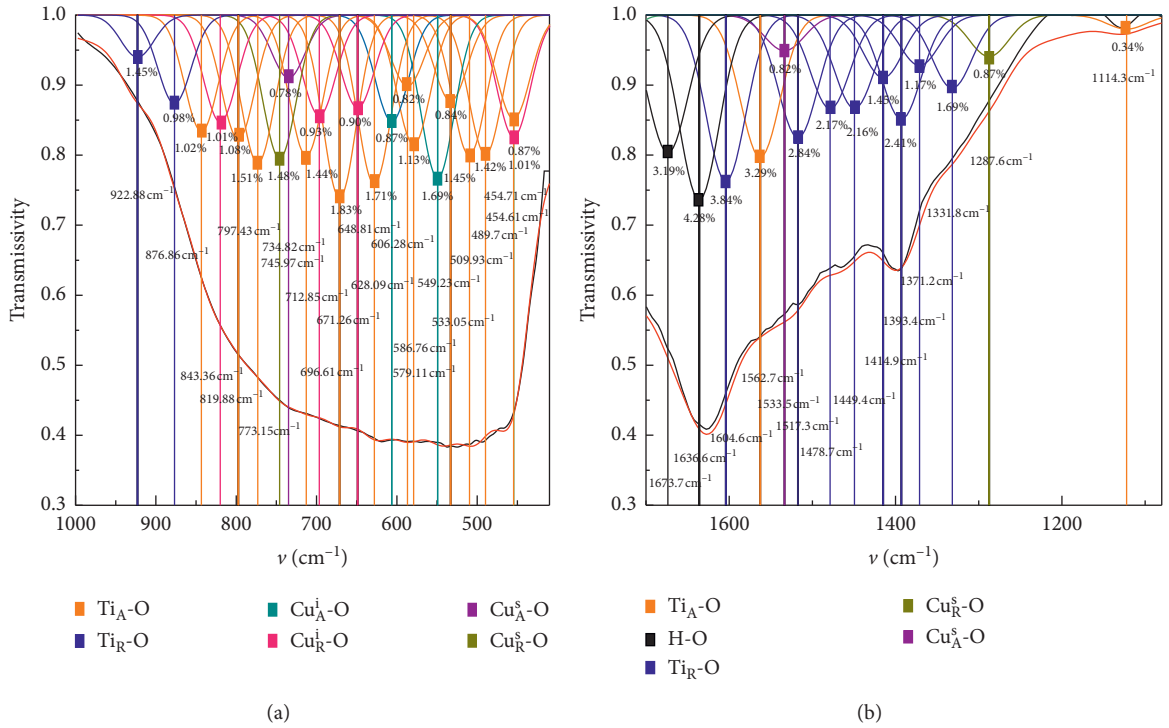

Figure 7: Infrared spectra of the 5 mol% Cu-doped TiO_2 samples at calcination temperature (550°C). (a) 400 cm^{-1}~1000 cm^{-1}; (b) 1000 cm^{-1}~1800 cm^{-1}.

Table 6: Infrared spectra of the 5 mol%Cu-doped TiO_2 samples with the content and vibrational frequency of valence bonds.

The type of bond	Content (%)	Vibrational frequency (cm^{-1})
Ti_A-O	18.75	1562.7, 1114.3, 843.36, 797.43, 773.15, 712.85, 671.26, 628.09, 586.76, 579.11, 533.05, 509.93, 489.7 and 454.71
Ti_R-O	20.11	1604.6, 1517.3, 1478.7, 1449.4, 1414.9, 1393.4, 1371.2, 1331.8, 922.88, and 876.86
H-O	7.47	1673.7 and 1636.6
Cu^i_A-O	2.56	606.28 and 549.23
Cu^i_R-O	3.9	819.88, 696.61, 648.81, and 454.61
Cu^s_A-O	1.55	1533.5 and 734.82
Cu^s_R-O	2.35	1287.6 and 745.97

The lattice parameters of undoped and Cu-doped samples are calculated from the XRD patterns. The lattice parameters remain unchanged, independent of Cu^{2+} content. This evidently considered that a greater portion of the Cu^{2+} ions is well-incorporated into the anatase and rutile TiO_2 lattice. The content of rutile increased obviously after Cu doping. This is indicated that the addition of Cu obviously promoted the transformation from anatase phase to rutile phase.

Figure 8 is the TEM diagram of sintering at 550°C with 5%Cu-doped TiO_2. According to Figure 8(a), the powder particles did not exceed 50 nm when the 5 mol%Cu-doped TiO_2 samples were sintered at 550°C. In addition, the agglomeration samples were serious, which made many small particles formed into large particles. Figure 8(b) shows that the stripes of different periods and orientations overlapped each other to form the Moiré patterns [36, 37]. In addition, the diffraction patterns of the Moiré image were slightly different from that of the matrix. It explains that the stretching vibration frequencies were changed by the Cu replaced Ti position and the Cu atoms mixed into interstitial sites in the TiO_2 lattice. The Cu-doped TiO_2 sample is characterized by FT-IR and TEM and calculated by electronegativity principle, and the theoretical calculation is consistent with the experimental results.

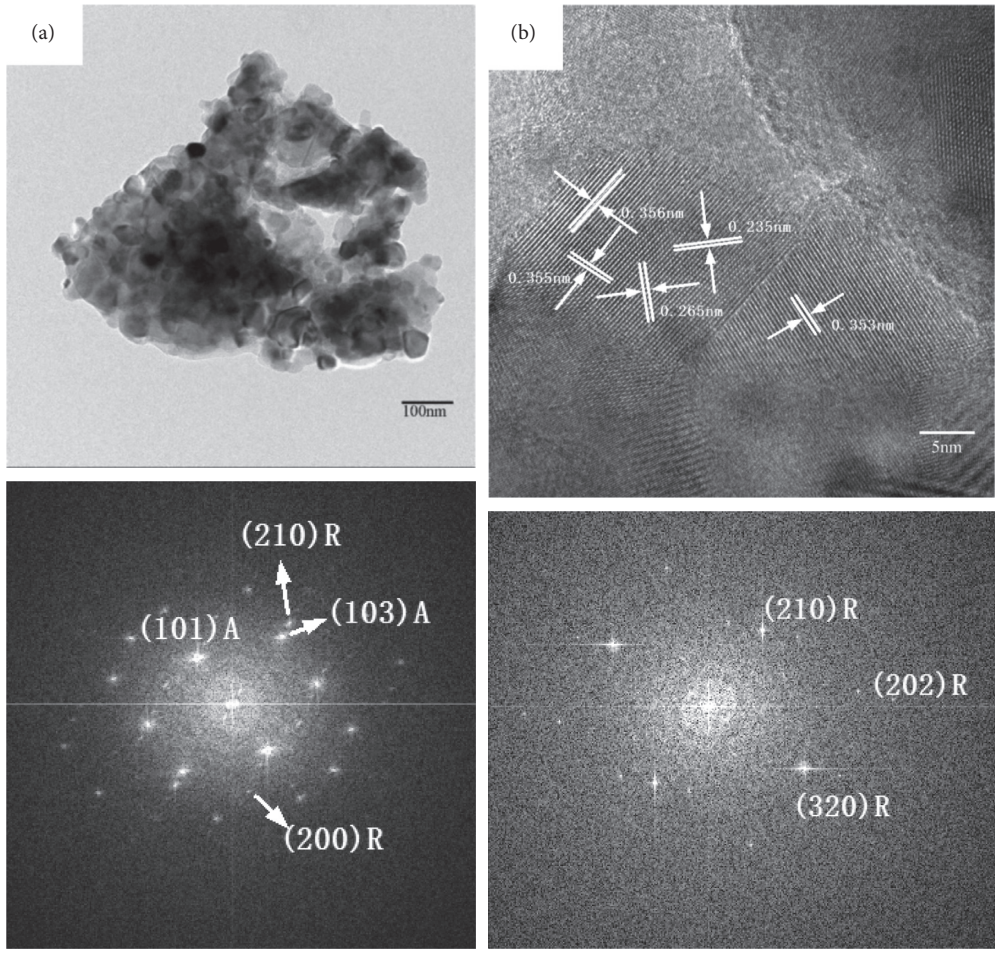

Figure 8: The TEM images of 5 mol% Cu-doped TiO_2.

4. Conclusion

The XRD phase analysis shows that the lattice parameters have not changed after Cu incorporation. In addition, the content of rutile increased obviously after Cu doping. This is indicated that the addition of Cu obviously promoted the transformation from anatase phase to rutile phase.

By all and low wavenumber section of infrared spectroscopy, we find that when the doping amount of Cu is 2.5 mol%, the content of Ti_A-O bonds is decreased by 2.64%, the content of Ti_R-O is increased by 2.26%, and the content of H-O bond is slightly changed. When the doping amount of Cu is 5 mol%, the content of Ti_A-O decreased by a further 2.48%, the content of Ti_R-O increased by a further 1.55%, the content of $Cu^i{}_A$-O increased by a further 1.58%, the content of $Cu^i{}_R$-O increased by a further 2.56%, the content of $Cu^s{}_A$-O decreased by a further 0.57%, the content of $Cu^s{}_R$-O increased by a further 1.01%, and the content of H-O bond is slightly changed. It quantitatively proved that the addition of Cu promoted the transformation from anatase phase to rutile phase. The incorporation of Cu has no effect on H-O bonds. When the doping amount of Cu is 2.5 mol%, the conversion efficiency is 2.26%. When the doping amount of Cu is 5 mol%, the conversion efficiency is 1.55%. This is explained that Cu atoms were more easily to be doped into rutile phase. The efficiency is that the quoted values refer to increases in the percentage content of rutile.

Data Availability

The data used to support the findings of this study are available from the corresponding author upon request.

Conflicts of Interest

The authors declare that they have no conflicts of interest.

Acknowledgments

This work was financially supported by National Natural Science Foundation of China (51362017) and Special Projects for Major Plans of Yunnan Province (Grant Nos. 2019ZE001 and 2018ZE005).

References

[1] X. Chen and S. S. Mao, "Titanium dioxide nanomaterials: synthesis, properties, modifications, and applications," *Chemical Reviews*, vol. 107, no. 7, p. 2891, 2007.

[2] J.-Y. Chen, J.-K. Yan, and G.-Y. Gan, "The effect of Cu doping on the transformation from rutile to anatase and Cu

occupation tendency in TiO_2 solid solution," *Journal of Spectroscopy*, vol. 2019, Article ID 6470601, 5 pages, 2019.

[3] Mohd, Faizan, Mohammad et al., "Anharmonic vibrational spectra and mode-mode couplings analysis of 2-aminopyridine," *Spectrochimica Acta, Part A. Molecular and Biomolecular Spectroscopy*, vol. 188, pp. 26–31, 2018.

[4] S. Livraghi, M. C. Paganini, E. Giamello et al., "Origin of photoactivity of nitrogen-doped titanium dioxide under visible light," *Journal of the American Chemical Society*, vol. 128, 2006.

[5] A. Kubacka, Fernández-García, C. Marcos, and Gerardo, "Advanced nanoarchitectures for solar photocatalytic applications," *Chemical Reviews*, vol. 112, no. 3, pp. 1555–1614, 2016.

[6] M. Miyauchi, H. M. Takashio, and H. Tobimatsu, "Photocatalytic activity of SrTiO3Codoped with nitrogen and lanthanum under visible light illumination," *Langmuir*, vol. 20, no. 1, p. 232, 2004.

[7] J. D. Bryan, S. A. S. M. Heald, and D. R. Gamelin, "Strong room-temperature ferromagnetism in Co2+-doped TiO_2 Made from colloidal nanocrystals," *Journal of the American Chemical Society*, vol. 126, no. 37, pp. 11640–11647, 2004.

[8] H. Li, Y. Wu, and J. Zhang, "CeO_2-TiO_2 catalysts for catalytic oxidation of elemental mercury in low-rank coal combustion flue gas," *Environmental Science & Technology*, vol. 45, no. 17, pp. 7394–7400, 2011.

[9] D. Fattakhova-Rohlfing, T. A. Zaleska, and T. Bein, "Three-dimensional titanium dioxide nanomaterials," *Chemical Reviews*, vol. 114, no. 19, pp. 9487–9558, 2014.

[10] A. P. Scott and L. Radom, "Harmonic vibrational frequencies: an evaluation of Hartree−Fock, Møller−Plesset, quadratic configuration interaction, density functional theory, and semiempirical scale factors," *The Journal of Physical Chemistry*, vol. 100, no. 41, pp. 16502–16513, 1996.

[11] S. Shaik, D. A. Shurki, and P. C. Hiberty, "Origins of the exalted b2uFrequency in the first excited state of benzene," *Journal of the American Chemical Society*, vol. 118, no. 3, pp. 666–671, 1996.

[12] R. Daghrir, D. P. Drogui, and D. Robert, "Modified TiO_2 for environmental photocatalytic applications: a review," *Industrial & Engineering Chemistry Research*, vol. 52, no. 10, pp. 3581–3599, 2013.

[13] V. Kumaeavel, S. Rhatigan, S. Mathew et al., "Mo doped TiO_2: impact on oxygen vacancies, anatase phase stability and photocatalytic activity," *Journal of Physics Materials*, vol. 3, no. 2, 2020.

[14] L. D. Trizio, R. Buonsanti, A. M. Schimpf et al., "Nb-doped colloidal TiO_2 nanocrystals with tunable infrared absorption," *Chemistry of Materials*, vol. 25, 2013.

[15] H. Zhang, J. R. Zong, and Y. Zhu, "Dramatic visible photocatalytic degradation performances due to synergetic effect of TiO_2 with PANI," *Environmental Science & Technology*, vol. 42, no. 10, pp. 3803–3807, 2008.

[16] C. Wei, Z. Peng, P. Zhang et al., "Study on process performance of N-doped porous titanium dioxide," *Iop Conference*, vol. 394, p. 394, 2018.

[17] R. D. Johnson, K. K. Irikura, R. N. Kacker, and R. Kessel, "Scaling factors and uncertainties for ab initio anharmonic vibrational frequencies," *Journal of Chemical Theory and Computation*, vol. 6, no. 9, p. 2822, 2010.

[18] S. Y. Chae, C. S. Lee, H. Jung et al., "Insight into charge separation in WO3/BiVO4 heterojunction for solar water splitting," *Acs Applied Materials & Interfaces*, vol. 9, 2017.

[19] M. Nolan, S. Callaghan, G. Fagas et al., "Silicon nanowire band gap modification," *Nano Letters*, vol. 7, no. 1, p. 34, 2010.

[20] Z. Liu, C. Y. Li, L. J. EYa, D. Zhao, and L. An, "TiO_2 photoanode structure with gradations in V concentration for dye-sensitized solar cells," *ACS Applied Materials & Interfaces*, vol. 3, no. 5, p. 1721, 2011.

[21] B. J. Zhao and G. W. Watson, "Intrinsic n-type defect formation in TiO_2: a comparison of rutile and anatase from GGA+U calculations," *The Journal of Physical Chemistry C*, vol. 114, no. 5, p. 2321, 2010.

[22] A. Mukhtar, N. B. S. Saqib, M. S. BabarRafiq et al., "A review on CO2 capture via nitrogen-doped porous polymers and catalytic conversion as a feedstock for fuels," *Journal of Cleaner Production*, vol. 277, p. 123999, 2020.

[23] B. Clemens, L. Sang, Z. Yixin et al., "TiO_2 nanoparticles as functional building blocks," *Chemical Reviews*, vol. 114, 2014.

[24] M. Z. Syazwani and S. Sreekantan, "Preparation and characterization of Cu loaded TiO? Nanotube Arrays and their photocatalytic activity," *Advanced Materials Research*, vol. 364, pp. 377–381, 2011.

[25] KhakiR. Mohammad et al., "Enhanced UV-Visible photocatalytic activity of Cu-doped ZnO/TiO_2 nanoparticles," *Journal of Materials Science Materials in Electronics*, vol. 29, 2018.

[26] G. Colón, M. Maicu, M. C. Hidalgo et al., "Cu-doped TiO_2 systems with improved photocatalytic activity," *Applied Catalysis B Environmental*, vol. 67, no. 1-2, pp. 41–51, 2006.

[27] Hengzhong, Zhang, Jillian et al., "Structural characteristics and mechanical and thermodynamic properties of nanocrystalline TiO_2," *Chemical Reviews*, vol. 114, no. 19, pp. 9613–9644, 2014.

[28] X. Wang, S. Olafsson, M. P. Sandstr et al., "Growth of $SrTiO_3$ thin films on LaAlO3(001) substrates; the influence of growth temperature on composition, orientation, and surface morphology," *Thin Solid Films*, vol. 360, no. 1-2, pp. 181–186, 2009.

[29] X. Chen, L. S. Shen, and S. S. Mao, "Semiconductor-based photocatalytic hydrogen generation," *Chemical Reviews*, vol. 110, no. 11, pp. 6503–6570, 2010.

[30] W. Su, Z. J. Zhang, and P. T. YingChen, "Surface phases of TiO_2 nanoparticles studied by UV Raman spectroscopy and FT-IR spectroscopy," *The Journal of Physical Chemistry C*, vol. 112, no. 20, pp. 7710–7716, 2008.

[31] Y. Li, K. Y. Meng, Y. H. JuQiu et al., "Copper-doped titanium dioxide bronze nanowires with superior high rate capability for lithium ion batteries," *ACS Applied Materials & Interfaces*, vol. 8, no. 12, pp. 7957–7965, 2016.

[32] A. Gao, M. Varshney, H. J. Shin et al., "Effect of Cu insertion on structural, local electronic/atomic structure and photocatalyst properties of TiO_2, ZnO and Ni (OH)2 nanostructures: XANES-EXAFS study," *Materials Chemistry and Physics*, vol. 191, 2017.

[33] K.-I. Hirota and M. Maeda, "Copper and nitrogen Co-doping effect on visible-light responsive photocatalysis of plasma-nitrided copper-doped titanium oxide film," *Journal of Materials Science and Chemical Engineering*, vol. 05, no. 12, pp. 52–62, 2017.

[34] H. Kim and M. W. Urban, "Molecular level chain scission mechanisms of epoxy and urethane polymeric films exposed to UV/H2O. Multidimensional spectroscopic studies," *Langmuir*, vol. 16, no. 12, pp. 5382–5390, 2000.

[35] J. Bloino, M. Biczysko, and V. Barone, "Anharmonic effects on vibrational spectra intensities: infrared, Raman, vibrational circular dichroism and Raman optical activity," *The Journal of Physical Chemistry A*, vol. 119, no. 49, 2015.

[36] V. Kumaravel, S. Rhatigan, S. Mathew et al., "Indium doped TiO 2 photocatalysts with high temperature anatase stability," *The Journal of Physical Chemistry C*, vol. 123, no. 34, 2019.

[37] I. Kriegel, J. C. Rodríguez-Fernández, D. V. Talapin, and J. Feldmann, "Tuning the excitonic and plasmonic properties of copper chalcogenide nanocrystals," *Journal of the American Chemical Society*, vol. 134, no. 3, pp. 1583–1590, 2012.